J Neurophysiol 128: 364–377, 2022.
First published July 13, 2022; doi:10.1152/jn.00483.2021

american physiological society

JNP JOURNAL OF NEUROPHYSIOLOGY

RESEARCH ARTICLE

Sensory Processing

Response of toadfish (*Opsanus tau*) utricular afferents to multimodal inputs

Loranzie S. Rogers,[1,2] Jacey C. Van Wert,[2] and Allen F. Mensinger[1,2]

[1]*Biology Department, University of Minnesota Duluth, Duluth, Minnesota and* [2]*Marine Biological Laboratory, Woods Hole, Massachusetts*

Abstract

The inner ear of teleost fishes is composed of three paired multimodal otolithic end organs (saccule, utricle, and lagena), which encode auditory and vestibular inputs via the deflection of hair cells contained within the sensory epithelia of each organ. However, it remains unclear how the multimodal otolithic end organs of the teleost inner ear simultaneously integrate vestibular and auditory inputs. Therefore, microwire electrodes were chronically implanted using a 3-D printed micromanipulator into the utricular nerve of oyster toadfish (*Opsanus tau*) to determine how utricular afferents respond to conspecific mate vocalizations termed boatwhistles (180 Hz fundamental frequency) during movement. Utricular afferents were recorded while fish were passively moved using a sled system along an underwater track at variable speeds (velocity: 4.0–12.5 cm/s; acceleration: 0.2–2.6 cm/s^2) and while fish freely swam (velocity: 3.5–18.6 cm/s; acceleration: 0.8–29.8 cm/s^2). Afferent fiber activities (spikes/s) increased in response to the onset of passive and active movements; however, afferent fibers differentially adapted to sustained movements. In addition, utricular afferent fibers remained sensitive to playbacks of conspecific male boatwhistle vocalizations during both passive and active movements. Here, we demonstrate in alert toadfish that utricular afferents exhibit enhanced activity levels (spikes/s) in response to behaviorally relevant acoustic stimuli during swimming.

NEW & NOTEWORTHY The inner ear of teleost fishes is composed of three paired multimodal otolithic end organs, which are sensitive to vestibular and auditory inputs. Previous studies investigating inner ear functions have primarily focused on the effects of unimodal stimuli; therefore, it remains unclear how otolithic end organs simultaneously encode multiple stimuli. Here, we show that utricular afferents remain sensitive to behaviorally relevant acoustic stimuli during swimming.

auditory; fish hearing; swimming; utricle; vestibular

INTRODUCTION

The vertebrate inner ear functions to maintain equilibrium and detect auditory stimuli. Across vertebrates, the vestibular function of the inner ear semicircular canals and the multimodal functions (vestibular and auditory) of the otolithic end organs have remained highly conserved since their evolution in teleost fishes. However, in concert with the change from an aquatic environment, terrestrial vertebrates have evolved specialized auditory sensors that allow for the detection of airborne acoustic stimuli (1–4). Thus, given that teleost fishes lack separate hearing organs, the multimodal otolithic end organs (saccule, utricle, and lagena) function as both linear accelerometers (vestibular) and act as the primary auditory sensors (5–8). Surprisingly, how fishes simultaneously integrate exafferent (externally derived) acoustic signals during reafferent (self-induced) vestibular stimulation continues to remain unclear.

Across vertebrates, it is widely agreed that auditory and vestibular efferent fibers function to modulate the gain of afferent hair cells and afferent encoding mechanisms (9–12). However, among anamniote vertebrates, the efferent system has been shown to differently modulate the inner ear auditory and vestibular systems and the mechanosensory lateral line. For example, inner ear efferents both excite (13–15) and inhibit (16–18) afferent fiber firing rates during efferent stimulation, whereas lateral line afferent hair cell signals are suppressed by neurons in higher-order central brain regions (19–22) and inhibited via efferent signaling at the periphery (23–27). However, these studies were primarily conducted in stationary, restrained, or fictive swimming animals, which does not recapitulate the motor output and motion-derived

Correspondence: L. S. Rogers (loranzie@uw.edu).
Submitted 1 November 2021 / Revised 13 July 2022 / Accepted 13 July 2022

sensory reafference experienced by free-swimming animals. Thus, it remains unclear how the multimodal inner ear in naturally behaving aquatic animals retain exafferent sensitivity during reafferent stimulation such as swimming.

The oyster toadfish (*Opsanus tau*) is a seasonally breeding fish that relies upon the production and reception of social acoustic signals to mediate reproductive encounters. Therefore, toadfish have served as a well-suited model for investigating the vestibular and auditory functions of the inner ear, including the semicircular canals (17, 28–30), saccule (31–33), and utricle (34–37). During late spring and summer, male toadfish establish nests in shallow waters off the eastern coast of the United States and acoustically attract gravid females via courtship vocalizations, termed boatwhistles, for reproduction (38–40). The ability of gravid female toadfish to detect the advertisement calls of courting males is critical to their reproductive success and has been shown to be mediated via the lateral line (41–43), saccule (32, 33), and utricle (37). However, female fish must also actively localize courting males, which is a motor-driven behavior that results in reafferent vestibular stimulation, to successfully reproduce. Therefore, female fish must maintain exafferent auditory sensitivity to male advertisement calls during active sound source localization. Yet, how this is accomplished remains to be known.

Investigations into neuronal exafference sensitivity during reafferent stimulation in free-swimming, naturally behaving fishes have yet to be conducted because of challenges with electrode stability, movement artifacts, and entanglement of tethers. Therefore, research has continued to rely upon fictive preparations, which provide valuable insights into the neural processes during the generation of motor signals but does not recreate the reafferent inputs experienced by free-swimming animals. However, recent advancements in three-dimensional (3-D) printed implantable micromanipulators (44) have allowed for long-duration chronic neural recordings in free-swimming fish following implants, which supports sustained neural recordings in animals exhibiting natural behaviors such as swimming (42).

Here, we use this recently developed implantable micromanipulator recording technique to test the hypothesis that the inner ear can simultaneously encode behaviorally relevant reafferent vestibular and exafferent auditory inputs. We conducted recordings from the toadfish utricle, an end organ that is primarily thought to serve a vestibular function (34, 35, 45–47) but also functions to transduce behaviorally relevant auditory inputs in toadfishes (37, 48). We compare utricular afferent firing rates during passive and active movements to determine the effect movement has on utricular activity levels. In addition, we compare how passive and active movements affect toadfish utricular afferents ability to encode conspecific vocalizations. We show that during passive and active movements, utricular afferent fibers increase their firing rates (spikes/s) during movement but remain sensitive to playbacks of behaviorally relevant auditory playbacks.

MATERIALS AND METHODS

Animal Husbandry

Adult toadfish (n = 15 females, n = 9 males; standard length 29.5 ± 1.9 cm; body mass 703.3 ± 119.5 g; means ± SD) were obtained from the Marine Biological Laboratory in Woods Hole, MA. Fish were kept in large flow-through seawater tanks and maintained at ambient water temperatures (20 ± 2°C). All experimental procedures conformed to NIH guidelines for animal care and use of animals and were approved by the Marine Biological Laboratory Institutional Animal Care and Use Committee under Protocol ID: 19-29.

Micromanipulator and Microwire Electrode Fabrication

Microwire electrodes were custom fabricated and integrated into a 3-D printed implantable micromanipulator (44). The micromanipulator (10 × 10 × 15 mm; 4.4 g) consisted of five parts (base, body, nut, screw drive, and electrode holder) that were fabricated with a Formlabs Form 2 3-D printer using clear photopolymer resin (Somerville, MA) (Fig. 1*A*). The electrodes were made by threading three insulated (250 μm outer diameter), silver-coated multistrand (seven wires per strand) copper wires (New England Wire Technologies, Lisbon, NH) through the body and electrode holder of the micromanipulator. The wire protruding from the back of the manipulator was soldered to insulated silver wires (320 μm) that terminated into an underwater connector and sealed with liquid electrical tape (Star brite, Fort Lauderdale, FL). Polyimide tubing (2 mm, 300 μm inner diameter) filled with conductive silver paint (GC Electronics, Rockford, IL) was used to join each multistrand wire to a 1 cm length of 10% platinum/iridium microwire (20 μm diameter, Sigmund Cohn, Mt. Vernon, NY). The three microwires were placed in a 3 mm segment of polyimide tubing (120 μm inner diameter) to maintain the electrode tips in close proximity, with ~2 mm of microwire protruding from the tubing. UV light-cured glue (Bondic; Aurora, Ontario, Canada) was used to insulate the final assembly and secure the polyimide tubing to the electrode holder. The impedance of all microwire electrodes was determined using an impedance-test unit (FHC, Inc.; Bowdoinham, ME), and only electrodes with an impedance between 0.7 and 1.8 MΩ were used in recordings.

Microwire Electrode Implant

During microwire electrode implants, toadfish were anesthetized by immersion in 0.005% tricaine solution and then immobilized with an intramuscular injection of 0.01% pancuronium bromide (600 μg/kg). Fish were placed within a custom stereotactic aquarium on a vibration isolation table, and a small medial incision through the dorsal musculature was made to expose the posterior dorsal surface of the skull. A small craniotomy was made lateral to the sagittal crest to expose the utricular nerve and otolith (Fig. 1*B*). The micromanipulator was secured with cyanoacrylate gel to the dorsal surface of the skull, and microwires were implanted by manually advancing the screw drive of the micromanipulator into the utricular nerve anterior to its projection from the anterior ramus of the VIII nerve (Fig. 1*B*, red regions). At this location, the utricular nerve has completely separated from the saccular nerve and contains only utricular fibers. Horizontal movements of the vibration isolation table confirmed that afferents were modulated by linear motion. The craniotomy was then sealed with cyanoacrylate gel, and the fascia and epidermis were sutured tightly around the micromanipulator to create a

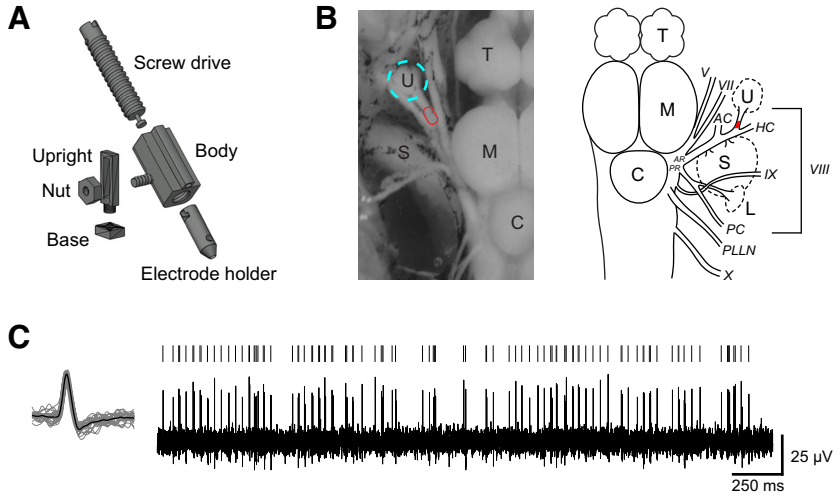

Figure 1. Utricular afferent neural recording and spike sorting paradigm. *A*: schematic of the three-dimensional (3-D) printed implantable micromanipulator used to implant microwire electrodes for chronic neural recordings. *B*, *left*: dorsal view of oyster toadfish brain and inner ear. The blue dashed circle highlights the utricle (U) while the red region indicates the implant position of microwire electrodes. *Right*: diagram of toadfish brain and inner ear: dorsal view showing the general location of nerve fibers and auditory regions. The red-colored area indicates the region where utricular (U) afferent recordings occurred. Roman numerals indicate cranial nerves. The schematic was based on Refs. 49 and 50. *C*: raw neural activity of a representative utricular afferent. Individual spikes were differentiated based on waveform template matching (*left*). For the representative waveform template, the gray lines indicate individual spikes, and the black line represents the mean waveform. Black horizontal lines represent the position of sorted spikes based on spike sorting analysis. AC, anterior canal; AR, anterior ramus; C, cerebellum; HC, horizontal canal; L, lagena; M, midbrain; PC, posterior canal; PLLN, posterior lateral line nerve; PR, posterior ramus; S, saccule; T, telencephalon.

watertight seal. Toadfish then were placed in the experimental arena and allowed to recover for 90 min, which is a sufficient amount of time for the tricaine solution and pancuronium injection to wash out (51).

Experimental Setup

The experimental arena consisted of a grounded circular fiberglass tank (350 L; 90 cm diameter × 55 cm; 50-cm water depth) placed on a 5-cm rubber mat on cinderblocks (40 × 20 × 10 cm) to minimize vibrations. An acrylic track (80 × 25 × 1.5 cm) with two parallel rails (80 × 4 × 1.5 cm) positioned 8 cm apart was elevated off the bottom of the arena by two acrylic supports (1.5 × 30 × 8 cm). An underwater speaker (Clark Synthesis AQ-339, Littleton, CO) was positioned upright on the bottom of the tank, ~30 cm perpendicular to the midpoint of the sled track (Fig. 2*A*). A USB camera (30 fps; 640 × 480 resolution; Svpro, New York, NY) was positioned 175 cm above the water surface to monitor fish movements.

Toadfish were allowed to swim spontaneously or were passively moved forward on a 3-D printed sled (12.5 × 7.5 × 2.5 cm, weight: 125 g). The sled was placed on the underwater track, and fish were affixed to the sled with plastic

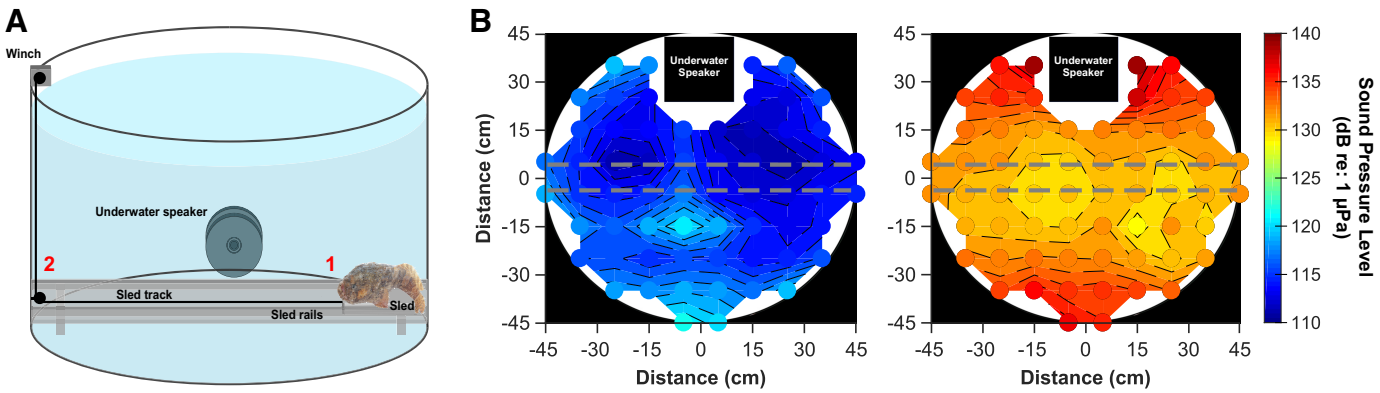

Figure 2. *A*: schematic of the experimental arena. Toadfish were passively moved (~75 cm) from position 1 to 2 while attached to a three-dimensional (3-D) printed sled (12.5 × 7.5 × 2.5 cm) on a track by a motorized winch system at variable speeds. Alternatively, fish freely swam throughout the experimental arena when the sled track was removed. An underwater speaker was positioned upright ~30 cm perpendicular from the midpoint of the sled track. Note that the schematic is not drawn to scale. *B*: sound pressure level (dB re: 1 μPa) maps of the experimental arena. *Left:* background sound pressure level (dB re: 1 μPa) map. *Right:* sound map during boatwhistle (425 ms duration; 180 Hz fundamental frequency) playbacks. All sound stimuli were presented at a sound pressure level of approximately 130 dB re: 1 μPa. Sound maps were constructed from sound pressure level (dB re: 1 μPa) measurements made at 62 points throughout the experimental arena 12.5 cm from the bottom (37.5 cm water depth). Gray dashed lines indicate the position of the sled rails, which were located 9.5 cm from the bottom (40.5 cm water depth) and guided the affixed toadfish during passive sled movement.

electrical ties around their mid-section. A custom-fabricated R/C motorized (Uxcell, Hong Kong) winch system, with monofilament as the cable, was secured to the upper rim of the tank opposite the fish's initial position and was used to move the fish/sled forward at three speeds [slow (5.51 ± 0.85 cm/s, 0.46 ± 0.12 cm/s^2); velocity, acceleration; medium (7.91 ± 1.11 cm/s, 0.94 ± 0.20 cm/s^2); and fast (11.02 ± 1.06 cm/s, 1.71 ± 0.34 cm/s^2)]. The monofilament was threaded through an underwater pulley positioned at track level to ensure the sled maintained contact with the track during movement (Fig. 2*A*).

Acoustic Stimulus and Calibration

The underwater speaker connected to a mixer amplifier (Bosch Plena; Farmington Hills, MI) delivered the acoustic stimulus, which consisted of either a continuous 60 s pure tone (125, 150, 175, and 200 Hz) created with a function generator (Model: AFG1022; Tektronix Co. Ltd., Shanghai, China) or a playback of a field recorded male toadfish boatwhistle (180 Hz fundamental frequency; 425 ms duration) with a duty cycle of 0.425 s on followed by 3.575 s off. Prior to each trial, the sound pressure level (dB re: 1 μPa) of all underwater acoustic stimuli was measured throughout the experimental tank using a calibrated hydrophone [HTI-96-MIN, open-circuit voltage (OCV) with preamp battery = −165 dB re: 1 V/μPa; High Tech Inc., Long Beach, MS], which was positioned 12.5 cm from the bottom (37.5 cm water depth), and connected to a PowerLab data acquisition system (Model 8/35; ADInstruments Inc., Colorado Springs, CO). Underwater acoustic stimuli were calibrated by determining the root mean square (rms) voltage (V_{rms}) of the measured analog acoustic stimulus. Using a custom MATLAB (v. 2017; MathWorks Inc., Natick, MA) script, the measured V_{rms} values were converted to dB and then corrected for the open-circuit voltage (*Eq. 1*). The signal (V_{rms}) was scaled until the measured sound pressure level (dB re: 1 μPa) output from the speaker was 130 ± 2 dB re: 1 μPa along the length of the sled track (Fig. 2*B*)

$$\mathrm{dB_{rms}\ re:\ 1\ \mu Pa} = 20\mathrm{Log}_{10}(V_{rms}) - \mathrm{OCV}. \quad (1)$$

Experimental Protocol

Following a recovery period of at least 90 min, after the implanted fish was moved to the experimental tank, the microelectrode underwater connector was coupled to a waterproof tether (~3 m) that connected to a differential amplifier (×1,000; Dagan Corporation, Minneapolis, MN). The neural signal (Fig. 1*C*) was filtered (0.03–5 kHz), recorded using Spike2 software (v. 8; Cambridge Electronic Design Ltd., Cambridge, UK), and monitored and stored on a portable computer. Two of the three microwire electrodes from each implant were chosen for recording based on signal fidelity. Before conducting physiology experiments, individual spikes were discriminated for each implant recording session using Spike 2 (v. 8; Cambridge Electronic Design Ltd., Cambridge, UK) waveform template matching (Fig. 1*C*, *left*). If the utricular neural signal became lost or diminished during experimental testing, the screw drive of the micromanipulator was adjusted to reposition the electrodes. Once high fidelity utricular afferents were re-acquired, individual spikes were discriminated and characterized to determine if the same utricular unit(s) were maintained or if new unit(s) had been attained (44). If the same unit(s) were obtained, experimental trials were resumed; however, if new unit(s) were isolated all experimental trials were repeated. Throughout the manuscript, the number of animals and utricular fibers recorded is presented as (n = no. of animals, no. of fibers), and individuals are identified by TF#-letter indicating a different utricular fiber (e.g., TF1-A, TF1-B).

For the initial acoustic experiments, stationary toadfish (n = 3, 4; no. of animals, no. of fibers) were positioned in the center of the tank with the cone of the underwater speaker positioned lateral, and ~30 cm from the ipsilateral side of the implant. Stationary fish were exposed to 60 s of continuous pure tone acoustic stimuli (125–200 Hz in 25 Hz steps) and a minimum of 10 consecutive boatwhistle vocalization playbacks (425 ms duration; fundamental frequency = 180 Hz; duty cycle = 0.425/3.575 s on/off) while utricular neural activity was recorded. If the fish moved during these trials, it was re-positioned in the center of the tank before subsequent testing.

During passive movement trials, fish (n = 18, 33) were positioned on the far right of the tank (Fig. 2*A*, position 1) and 30 s of spontaneous utricular activity was recorded. Fish were then pulled across the tank (~ 75 cm) to the opposite side (Fig. 2*A*, position 2), and then spontaneous utricular afferent fiber activity was recorded for an additional 30 s. The fish/sled was pulled forward for a minimum of five trials at each speed, with a recovery period of 120 s between each trial. In addition, during the slow speed trials, utricular afferent fiber activity was recorded with and without boatwhistle playbacks. During the acoustical stimulus trials (n = 5–10/fish), 5 boatwhistle playbacks were presented pre- and postmovement; however, during transit, there was only time for one boatwhistle per track segment (initial, middle, and end) due to the duration of sled movements. The angle of the speaker relative to the midline of the anterior portion of the fish was approximately at 30° (premovement), 45°–75° (initial), 75°–105° (middle), 105°–135° (end), and 150° (postmovement) during playbacks. Alternatively, fish (n = 6, 6) were also allowed to freely swim throughout the experimental arena after the underwater track was removed, and neural activity was recorded with and without boatwhistle playbacks (n = 5/fish).

Particle Acceleration

The inner ear otolithic end organs of fishes contain dense calcium carbonate otoliths that rest on a sensory bed of hair cells and act as inertial accelerometers that are sensitive to local particle motion and respond to changes in linear acceleration induced by both self-motion and acoustic stimuli. It remains to be determined if oyster toadfish are sensitive to sound pressure (dB re: 1 μPa), which is transmitted via local particle motion (dB re: 1 m/s^2) generated by pressure wave-induced vibrations of the swim bladder when exposed to sound pressure signals; however, in recent studies in a closely related toadfish species, the plainfin midshipman (*Porichthys notatus*) have demonstrated sound pressure (dB re: 1 μPa) sensitivity (52, 53). Therefore, in addition to measuring the sound pressure levels (dB re: 1 μPa) of the acoustic

stimuli, particle acceleration levels (dB re: 1 m/s^2) for background conditions, passive movements (slow, medium, and fast), and boatwhistle playbacks were determined along the track using a calibrated waterproofed triaxial accelerometer [Model: W356A12/NC; Sensitivity: x = 10.47 mV/(m/s^2); y = 10.35 mV/(m/s^2); z = 10.29 mV/(m/s^2); PCB Piezotronics, Depew, NY]. The triaxial accelerometer was connected to a signal conditioner (Model: 482 C; PCB Piezotronics, Depew, NY) and monitored with a PowerLab data acquisition system running LabChart software (v. 8; ADInstruments, Colorado Springs, CO). Particle acceleration (dB re: 1 m/s^2) during passive movements was measured throughout the duration of movement while the accelerometer was attached to the sled at the position of the fish's head and pulled along the track at the three speeds (slow, medium, and fast). To determine particle acceleration levels (dB re: 1 m/s^2) for background conditions (i.e., no stimulus) and during boatwhistle playbacks, the accelerometer was made neutrally buoyant using polystyrene insulation sheathing (41) and suspended at the position of the fish before movement (premovement), at the midpoint of each track segment (initial, middle, and end) and after movement (postmovement). All measurements were made ~6 cm above the track to correspond with the utricle location during passive movement trials. Background particle acceleration levels (dB re: 1 m/s^2) were determined over a 10-s interval when all stimuli were absent, whereas particle acceleration levels (dB re: 1 m/s^2) of boatwhistle playbacks were determined throughout the duration of the stimulus epoch at each track segment. Particle acceleration (dB re: 1 m/s^2) was calculated with a custom MATLAB (v. 2017; MathWorks Inc., Natick, MA) script, where the root mean square (rms) voltage (V_{rms}) values of each axis (x-, y-, and z-axes) were calibrated to the sensitivity of the accelerometer and used to calculate the magnitude of particle acceleration in the dB scale (*Eq. 2*) (54, 55) as follows:

$$\text{dB re: 1 m/s}^2 = 20\text{Log}_{10}(\sqrt{x^2 + y^2 + z^2}). \quad (2)$$

Kinematic Measurements

Toadfish kinematic measurements were made using custom software developed in MATLAB (v. 2017; MathWorks Inc., Natick, MA). Kinematic data were collected for all trials using overhead video recordings (30 fps; 640 × 480 resolution). Toadfish position was tracked manually by using the screw drive of the implanted micromanipulator as a reference point and then filtered with smoothening splines. Using positional data, instantaneous velocities (v; cm/s) and accelerations (a; cm/s^2) were determined using the following equations:

$$v = (s_{i+1} - s_i)/(t_{i+1} - t_i) \quad (3)$$

$$a = (v_{i+1} - v_i)/(t_{i+1} - t_i), \quad (4)$$

where velocity (v; cm/s) is equal to the change in fish position ($s_{i+1} - s_i$) over a given time period ($t_{i+1} - t_i$), whereas linear acceleration (a; cm/s^2) is equal to the change in velocity ($v_{i+1} - v_i$) over a given time period ($t_{i+1} - t_i$). The magnitude of velocities (v; cm/s) and accelerations (a; cm/s^2) during self-generated movements were determined using the following equations:

$$v = \sqrt{\left(\frac{(x_{i+1} - x_i)}{(t_{i+1} - t_i)}\right)^2 + \left(\frac{(y_{j+1} - j)}{(t_{i+1} - t_i)}\right)^2} \quad (5)$$

$$a = \sqrt{\left(\frac{(v_{xi+1} - v_{xi})}{(t_{i+1} - t_i)}\right)^2 + \left(\frac{(v_{yj+1} - v_{yj})}{(t_{i+1} - t_i)}\right)^2} \quad (6)$$

where the magnitude of the velocity (v; cm/s) is the root mean square of the toadfish position along the x- and y-axes over time ($t_{i+1} - t_i$), whereas acceleration (a; cm/s^2) is the root mean square of the toadfish velocity (v; cm/s) along the x- and y-axes over time.

Analyses

During experimental recording trials, neural activity and acoustic stimuli were recorded using a CED Micro 1401 data acquisition unit, and Spike2 software (v. 8; Cambridge Electronic Design Ltd., Cambridge, UK). Individual utricular afferent fibers were discriminated offline using Spike2 (v. 8; Cambridge Electronic Design Ltd., Cambridge, UK) via a systematic comparison of spike features including waveform amplitude and duration via template matching. Afferent fiber firing rates (spikes/s) were analyzed using MATLAB (v. 2017; MathWorks Inc., Natick, MA). All data passed normality testing except for particle acceleration level (dB re: 1 m/s^2) measurements, which were analyzed using nonparametric tests.

Spontaneous firing rates (spikes/s) were determined as the number of spikes over a 10-s interval when all sensory stimuli were absent while firing rates (spikes/s) during movements were calculated as the number of spikes throughout the duration of movement and boatwhistle-evoked firing rates (spikes/s) were determined as the number of spikes during each stimulus epoch (425 ms duration). The coefficient of variation (CV), which is a dimensionless ratio of the standard deviation to mean interspike interval duration, was also determined for each fiber. Utricular fibers were then characterized as regular (normal distribution; CV < 0.4) or irregular (non-normal distribution; CV ≥ 0.4) based on their interspike interval histograms and CV values.

During passive movement trials when the acoustic stimulus was absent, utricular fibers were classified as either slow adapting, which was characterized by an initial increase in firing followed by a sustained response above spontaneous rates (spikes/s) throughout movement, or fast adapting, which displayed peak firing rates (spikes/s) within one second of movement followed by a return to ±5% of baseline rates during the remainder of passive movement. During passive sled movements, linear models were constructed to determine if there was a significant ($P < 0.05$) correlation between utricular afferent activity levels (spikes/s) and the velocity (cm/s) and acceleration (cm/s^2) of passive movements (slow, medium, and fast). To determine differences between particle acceleration levels (dB re: 1 m/s^2) during passive movements (slow, medium, and fast) in the absence of acoustic stimuli, a Kruskal–Wallis one-way ANOVA was conducted followed by a Dunn–Holm post hoc test.

To determine if there were significant differences in utricular fiber activities (spikes/s) in response to boatwhistle playbacks while stationary, and during slow sled movements with or without boatwhistle playbacks, a one-way repeated-

measures ANOVA followed by pairwise comparison post hoc testing with a Holm correction was conducted. In addition, a Kruskal–Wallis one-way ANOVA followed by a Dunn–Holm post hoc test compared particle acceleration levels (dB re: 1 m/s^2) during boatwhistle playbacks while stationary and during passive movement and background conditions.

During swimming, a linear model correlated swimming accelerations with firing rates (spikes/s). In addition, a one-way repeated-measures ANOVA followed by pairwise comparison post hoc testing with a Holm correction compared spontaneous firing rates (spikes/s) to the firing rates of fish while stationary during boatwhistle playbacks and while swimming in the presence and absence of boatwhistle playbacks.

For stationary acoustic trials, a Student's t test was conducted to compare spontaneous and evoked (pure tone and boatwhistle) utricular afferent firing rates (spikes/s). Phase-locking analysis of utricular fibers in response to pure tones and boatwhistle playbacks was determined by calculating the synchronization coefficient, R, according to Goldberg and Brown (56) (*Eq. 7*) as follows:

$$R = \frac{1}{n}\sqrt{\left(\sum \cos(\theta_i) \times n_{\theta_i}\right)^2 + \left(\sum \sin(\theta_i) \times n_{\theta_i}\right)^2}. \quad (7)$$

Here, phase angle (θ_i) ranges from 0 to 2π, n_{θ_i} is equal to the number of discharges at a given θ_i, and n represents the total number of discharges occurring between 0 and 2π. A minimum of 350 action potentials were used for phase-locking analysis. Strong phase-locking was defined as $R > 0.5$, whereas weak phase-locking was represented by $R \leq 0.5$ (56). Given that a small sample size (n) may misrepresent R, the Rayleigh statistic (Z), which is a combined measure of n and R defined as $n \times R^2$, was calculated to determine whether R was statistically significant ($Z > 6.91$; $P < 0.001$) (57, 58). Phase-locking in response to boatwhistle playbacks was conducted relative to the tonal portion of the call (Fig. 3*C*). Phase-locking was determined relative to the stimuli's fundamental frequency for all acoustic stimuli. Phase-locking analysis in response to boatwhistles playbacks during slow passive movements was conducted before movement, at the track's initial, middle, and end segments, and postmovement. Phase histograms, which were binned in 3° increments, for each position, were then pooled across trials, and R and Z were determined.

RESULTS

The activity of 40 utricular afferent fibers was recorded from 24 toadfish. All units exhibited spontaneous firing rates ranging from 2.8 to 76.7 spikes/s (22.7 ± 15.5 spikes/s; means ± 1 SD). The units were comprised predominately of irregular-type fibers (n = 35 fibers; CV > 0.4) with the remainder of the units displaying regular firing patterns (n = 5 fibers; CV < 0.4).

To ensure that the newly developed micromanipulator did not affect utricular afferent sensitivity, several fish (n = 3, 4; no. animals, no. fibers) were positioned 30 cm from the underwater speaker, and neural activities in response to pure tones (125, 150, 175, and 200 Hz) were recorded. The evoked firing rates (spikes/s) of all recorded fibers significantly increased (Student's t test, $P < 0.05$) above spontaneous resting rates (spikes/s) in response to acoustic stimuli. In addition, these fibers displayed significant phase-locking in response to acoustic stimuli while stationary. Figure 3*A* illustrates the phase-locking analysis for utricular fiber TF5-A,

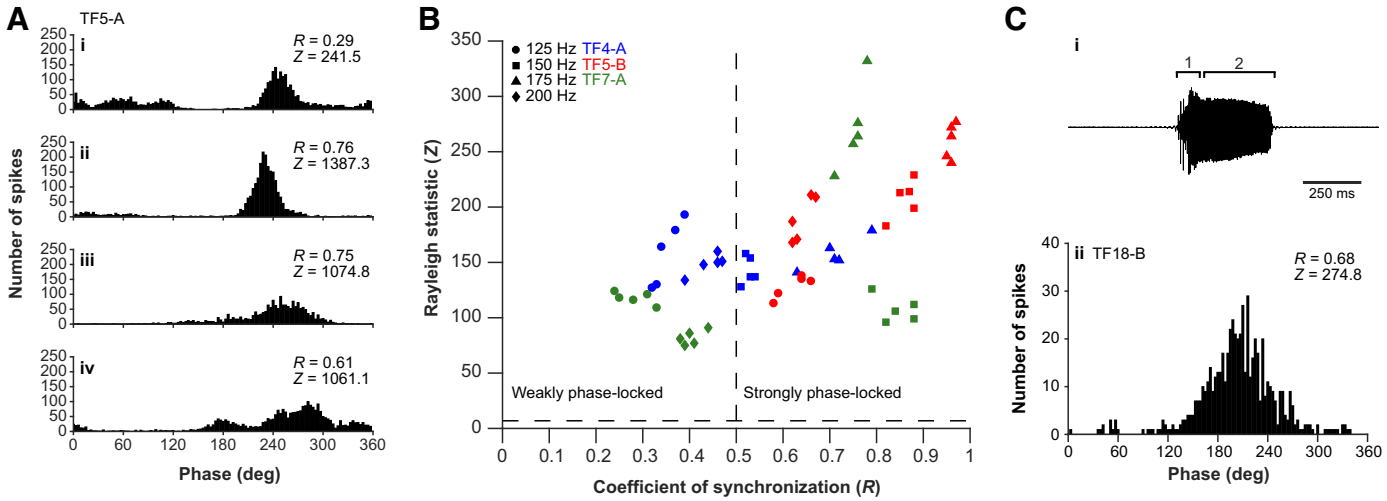

Figure 3. Utricular afferent response to pure tone stimuli (*A* and *B*) and boatwhistle playbacks (*C*). All auditory stimuli were presented at a sound pressure level of 130 ± 2 dB re: 1 µPa. *A*: phase histograms show the total number of spikes versus one sinusoidal cycle for utricular afferent fiber TF5-A in response to pure tone stimuli [*i*) 125 Hz, *ii*) 150 Hz, *iii*) 175 Hz, and *iv*) 200 Hz]. *B*: Rayleigh statistic (Z) is plotted against the coefficient of synchronization (R) for three toadfish afferent fibers in response to 125 (○), 150 (□), 175 (Δ), and 200 Hz (◊) pure tone stimuli. Individual afferent fibers are plotted with a different color (red, blue, or green). The vertical dashed line (R = 0.5) indicates the divide between weak ($R \leq 0.5$) and strong ($R > 0.5$) phase-locking, while the horizontal line (Z = 6.91) represents the divide between significant ($Z > 6.91$, $P < 0.001$) and nonsignificant ($Z < 6.91$, $P > 0.001$) phase-locking. *C*: utricular afferent fibers significantly phase-lock to boatwhistle playbacks. *i*) Waveform of boatwhistle vocalization (425 ms, 180 Hz fundamental frequency), where 1 represents the initial broadband grunt segment, and 2 represents the tonal portion of the call. *ii*) Phase histogram of fiber TF18-B in response to boatwhistle playbacks (n = 10). All phase histograms in response to pure tones and boatwhistle playbacks were binned in 3° increments, and a minimum of 350 action potentials were used during phase-locking analysis.

which strongly and significantly phase-locked to 150, 175, and 200 Hz pure tones (150 Hz: R = 0.76, Z = 1,387.3; 175 Hz: R = 0.75, Z = 1,074.8; 200 Hz: R = 0.61, Z = 1,061. 1) and weakly phase-locked to 125 Hz (R = 0.29, Z = 241.5). Figure 3*B* displays the phase-locking responses of three additional utricular afferents (TF4-A, TF5-B, and TF7-A) in response to pure tones. Utricular afferents also responded to conspecific boatwhistle vocalization playbacks (Fig. 3*Ci*) by significantly increasing (Student's t test, $P < 0.05$) their firing rates (spikes/s) during stimulus presentation and exhibiting strong ($R > 0.5$) and significant phase-locking ($Z > 6.91$, $P < 0.001$) to the tonal portion of the boatwhistle vocalization playback (Fig. 3*Cii*).

Utricular Activity during Passive Movement

The duration (s), velocity (cm/s), and acceleration (cm/s^2) of passive movements were inversely correlated to toadfish body mass (range 482.0–941.4 g), with heavier fish traveling slower along the track resulting in reduced velocities (cm/s) and accelerations (cm/s^2). Regardless, all afferent fibers (n = 18, 33) tested increased their firing rates (spikes/s) at the onset of movement. During passive movements, 15 utricular afferent fibers from 10 toadfish were maintained through all three speeds (slow, medium, and fast: n = 5 trials/speed). Figure 4*A* displays the spontaneous and passive movement evoked activities (spikes/s) of the utricular fibers (n = 10, 15)

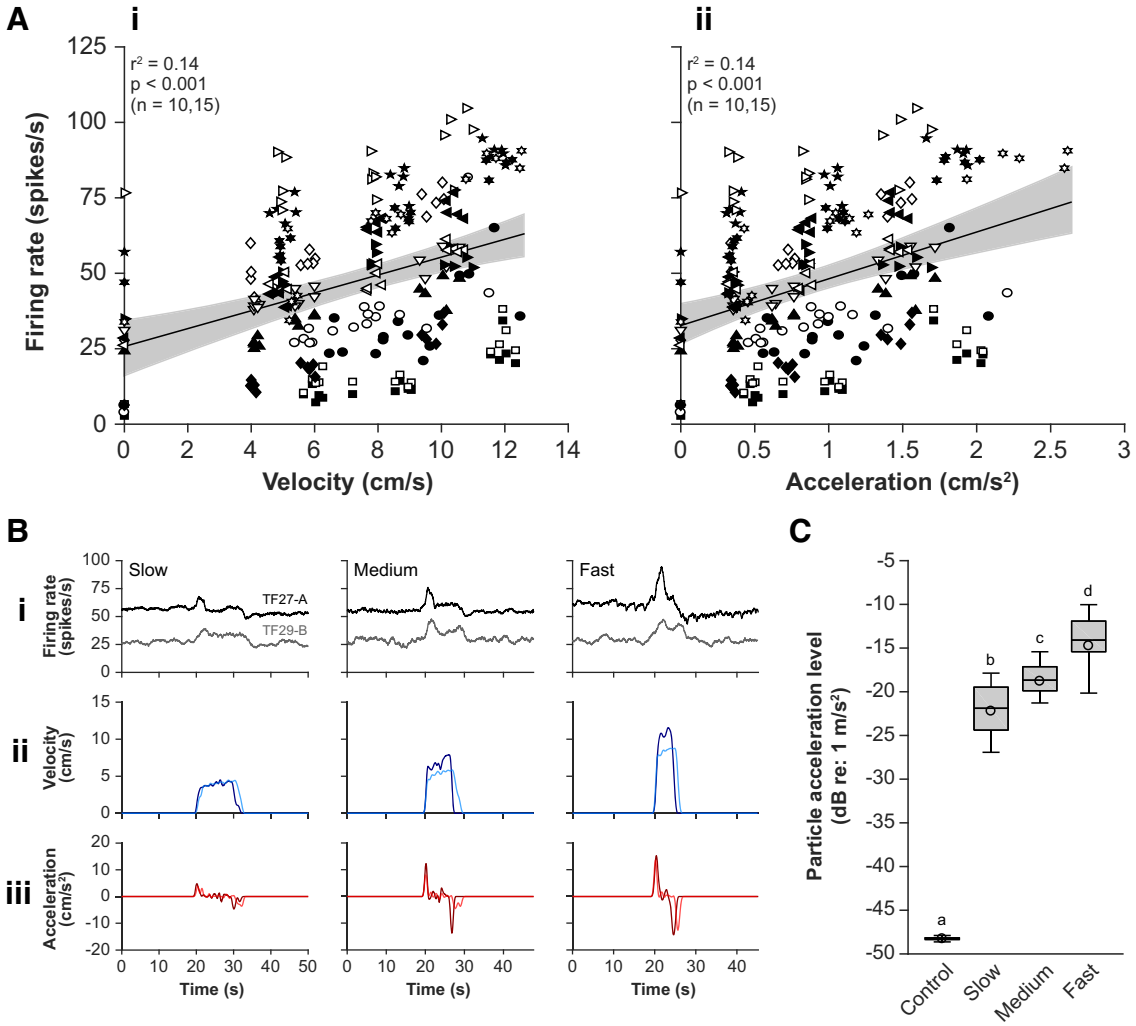

Figure 4. Utricular afferent firing rates (spikes/s) increased during passive sled movements. *A*: utricular afferent fiber firing rates (spikes/s) plotted against the mean linear *i*) velocity (cm/s) and *ii*) acceleration (cm/s^2) for each passive movement trial (n = 225). The mean spontaneous fiber activity (spikes/s) for each utricular fiber is plotted at 0 velocity (cm/s) and acceleration (cm/s^2), respectively. The different symbols represent the utricular afferent firing rates (spikes/s) from individual afferent fibers. The black line represents the best fit line, while the shaded region represents the 95% confidence interval. The number in the parentheses indicates the number of fish and afferent fibers recorded during slow, medium, and fast passive sled movements. *B*: utricular afferent firing rates (spikes/s) of a fast (TF27-A; dark colors) and slow (TF29-B; light colors) adapting fiber before, during, and after passive sled movement at three speeds (slow, medium, and fast). Each panel (from *top* to *bottom*) represents the *i*) utricular afferent firing rates (spikes/s) during passive sled movement, *ii*) instantaneous linear velocities (cm/s), and *iii*) accelerations (cm/s^2). *C*: boxplots of particle acceleration levels (dB re: 1 m/s^2) during slow, medium, and fast passive sled movements. Control indicates the background particle acceleration levels (dB re: 1 m/s^2) within the experimental arena when all stimuli were absent. The line within the box represents the median and the mean of the data by an open circle. The box extends to the 25th and 75th percentile, while the upper and lower tails extend to the 90th and 10th percentiles, respectively. Different letters indicate significantly different particle acceleration levels (Dunn–Holm, $P < 0.05$).

that were held throughout all three speeds plotted against mean linear *i*) velocity (cm/s) and *ii*) acceleration (cm/s^2) for all trials conducted (n = 225). During passive movements, there was a significant ($P < 0.001$) positive correlation between utricular fiber firing rates (spikes/s) and passive movement velocity (r^2 = 0.14) and acceleration (r^2 = 0.14). However, the sustained firing patterns of utricular afferent fibers varied over the duration of passive movement. The majority (n = 28) of the 33 afferent fibers tested during passive movements were slow adapting and exhibited a phasic response at the onset of movement with a modest decrease in firing rate that was sustained above baseline throughout passive movements. In contrast, fast adapting fibers (n = 5) exhibited phasic response patterns, which increased firing rates during the initial phase of acceleration increase before returning to ±5% of baseline activity levels throughout the duration of passive movement. Figure 4*B* illustrates the neural activity (spikes/s) of a representative fast (TF27-A) and slow (TF29-B) adapting fiber during slow, medium, and fast passive movements. In addition, because the inner ear transduces changes in linear acceleration, particle acceleration levels (dB re: 1 m/s^2) during slow, medium, and fast passive sled movements were compared with background particle acceleration levels (dB re: 1 m/s^2). Based on these measurements, it was observed that particle acceleration levels (dB re: 1 m/s^2) significantly increased (Kruskal–Wallis ANOVA, $\chi^2_{3,3703}$ = 2803, $P < 0.001$) above median background levels (control; median = −48.27 dB re: 1 m/s^2) during slow (median = −21.89 dB re: 1 m/s^2), medium (median = −18.68 dB re: 1 m/s^2), and fast (median = −14.09 dB re: 1 m/s^2) passive sled movements, and that particle acceleration levels (dB re: 1 m/s^2) significantly increased as passive sled movement speed increased (Fig. 4*C*, Dunn–Holm, $P < 0.001$).

The activities (spikes/s) of utricular afferent fibers (n = 12, 22) were also determined during slow passive movements (5.51 ± 0.85 cm/s, 0.46 ± 0.12 cm/s^2) in response to boatwhistle playbacks (130 ± 2 dB re: 1 μPa; Fig. 2*B*). Figure 5, *A* and *B* illustrates the utricular activity (spikes/s) of a representative slow (TF18-B) and fast (TF26-A) adapting fiber before, during, and after slow passive movement in the *i*) absence and *ii*) presence of boatwhistle playbacks. Both afferents increased their firing rates (spikes/s) in response to passive movements (Fig. 5, *Ai* and *Bi*), and boatwhistle playbacks while stationary and during passive movements (Fig. 5, *Aii* and *Bii*). In addition, both fibers displayed strong ($R > 0.50$) and significant ($Z > 6.91$, $P < 0.001$) phase-locking to the tonal portion of boatwhistle vocalization playbacks throughout passive movement (Fig. 5, *Aiii* and *Biii*). Figure 5*C* illustrates the response (spikes/s) of all fibers (n = 12, 22), which displayed similar neural responses to the two utricular fibers (TF18-B and TF26-A) illustrated in Fig. 5, *A* and *B*. Firing rates (spikes/s) significantly increased (one-way repeated-measures ANOVA, $F_{3,315}$ = 142.8, $P < 0.001$) in response to boatwhistle playbacks while stationary, and during slow passive movements when boatwhistle playbacks were absent and present. In addition, utricular fiber firing rates (spikes/s) in response to boatwhistle playbacks during slow passive movements were significantly greater ($P < 0.001$) than utricular afferent firing rates (spikes/s) in response to boatwhistle playbacks while stationary and during slow passive movements when acoustic stimuli were absent (Fig. 5*C*). Similarly, particle acceleration (dB re: 1 m/s^2), which is the acoustic signal most fish are sensitive to, significantly increased (Kruskal–Wallis ANOVA, $\chi^2_{3,2479}$ = 1821, $P < 0.001$) above median background particle acceleration levels (control = −48.27 dB re: 1 m/s^2) when stimuli were present (Fig. 5*D*). In addition, the particle acceleration levels (dB re: 1 m/s^2) of boatwhistle playbacks while stationary (boatwhistle; median = −15.47 dB re: 1 m/s^2) and during slow passive movements (boatwhistle + slow; median = −15.73 dB re: 1 m/s^2) were significantly greater (Dunn–Holm, $P < 0.001$) than the particle acceleration levels (dB re: 1 m/s^2) of slow passive movements (slow; median = −21.89 dB re: 1 m/s^2) (Fig. 5*D*).

Utricular Response during Swimming

The activity levels (spikes/s) of utricular afferent fibers (n = 6, 6) were recorded during swimming events, ranging from 2 to 15 s durations, covering distances of 15–120 cm, at mean linear accelerations ranging from 0.8 to 29.8 cm/s^2. Like passive movements, there was a significant ($P < 0.001$) positive correlation (r^2 = 0.57) between utricular afferent fiber firing rates (spikes/s) and the mean linear acceleration of active swimming movements (Fig. 6). Utricular afferent fibers (n = 6, 6) also retained auditory sensitivity to playbacks of conspecific boatwhistles during swimming (Fig. 7). Figure 7, *A* and *B* illustrates the activity levels (spikes/s) of utricular afferent fibers TF17-B and TF32-A, respectively, in response to boatwhistle playbacks while stationary and swimming. Two brief swims were monitored in Fig. 7*A*, with peak velocities of 6.1 and 6.3 cm/s and accelerations of 11.3 and 16.8 cm/s^2. Although TF17-B was stationary, boatwhistle playbacks evoked spike rates (85.1 ± 2.0 spikes/s) that significantly increased (Student's t test, $P < 0.001$) above spontaneous rates (44.4 ± 1.4 spikes/s). During self-generated swimming, rates increased to 59.2 ± 1.7 spikes/s and continued to increase during boatwhistle playbacks to 89.5 ± 6.1 spikes/s (Fig. 7*A*, gray bar). Similarly, the firing rates (spikes/s) of fiber TF32-A in Fig. 7*B* significantly increased (Student's t test, $P < 0.001$) above baseline (15.4 ± 1.3 spikes/s) to 53.9 ± 0.8 spikes/s in response to boatwhistle playbacks while stationary. During swimming, rates increased to 27.8 ± 8.0 spikes/s when acoustic stimuli were absent and to 47.8 ± 4.3 spikes/s during boatwhistle playbacks (Fig. 7*B*, shaded gray bar). Similarly, firing rates (spikes/s) across all utricular fibers (n = 6, 6) significantly increased (one-way repeated measures ANOVA, $F_{3,111}$ = 59.86, $P < 0.001$) in response to swimming events and conspecific boatwhistle playbacks while stationary and during swimming (Fig. 7*C*). Across utricular afferent fibers, firing rates (spikes/s) during swimming events were significantly greater (P = 0.014) than evoked firing rates (spikes/s) in response to boatwhistle playbacks while stationary. Additionally, utricular afferent firing rates (spikes/s) in response to boatwhistle playbacks while swimming were significantly greater than swimming-evoked rates (P = 0.014) and boatwhistle-evoked rates while stationary ($P < 0.001$).

DISCUSSION

The otolithic end organs (saccule, utricle, and lagena) of the teleost inner ear function as linear accelerometers and particle motion detectors (5–8). Previous investigations into the teleost inner ear have primarily focused on the auditory

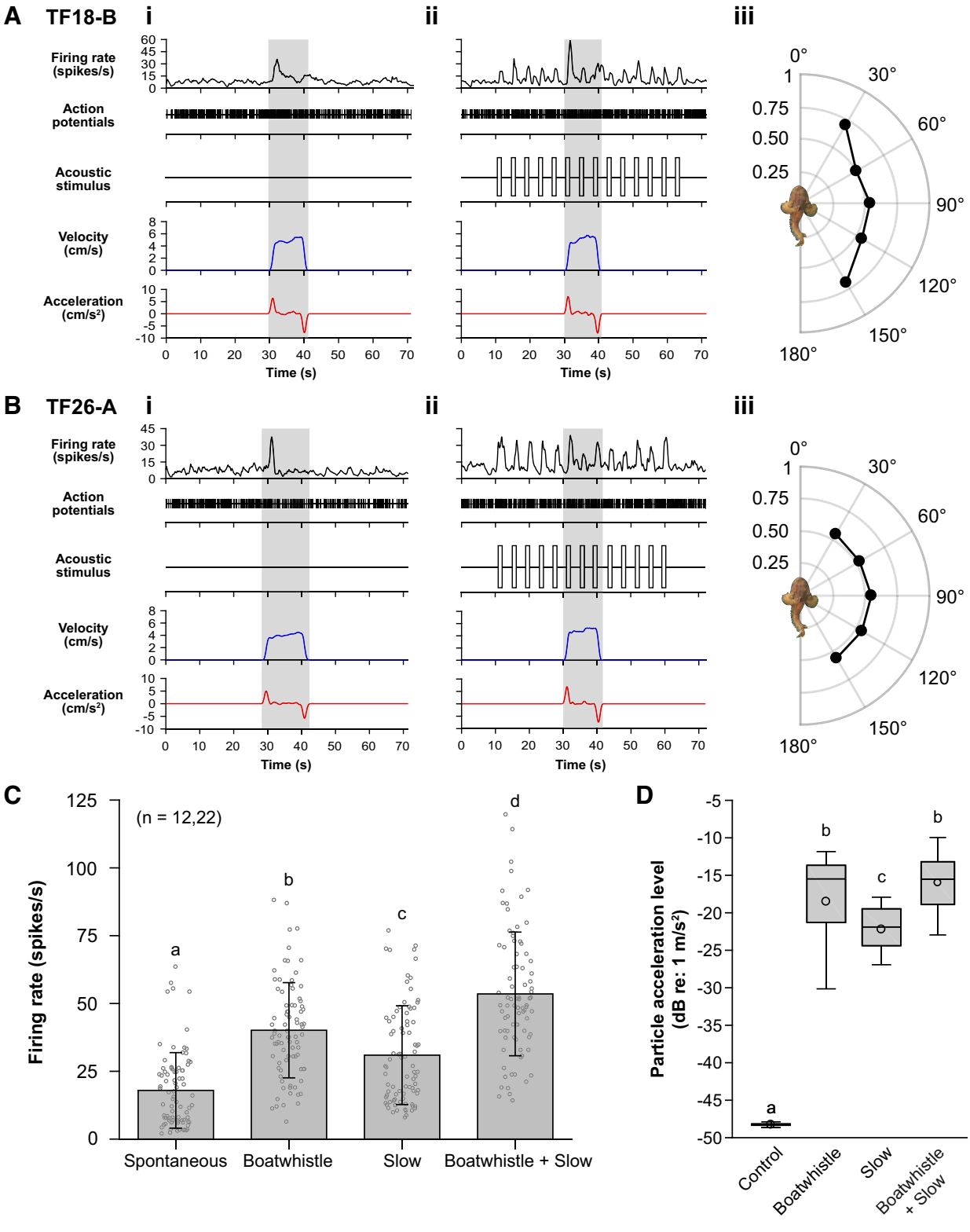

role of the otolithic end organs, with the saccule receiving the most attention (7). However, each otolithic end organ has a multimodal function and is sensitive to both auditory and vestibular inputs (34, 35, 37, 47, 48, 59). Therefore, the goal of this study was to conduct in vivo electrophysiology recordings from primary utricular afferent neurons in the toadfish during passive and active movements while presenting recordings of conspecific vocalizations to characterize the effect of movements on the detection of auditory stimuli. Here, we show that utricular afferent fibers exhibit robust

J Neurophysiol • doi:10.1152/jn.00483.2021 • www.jn.org

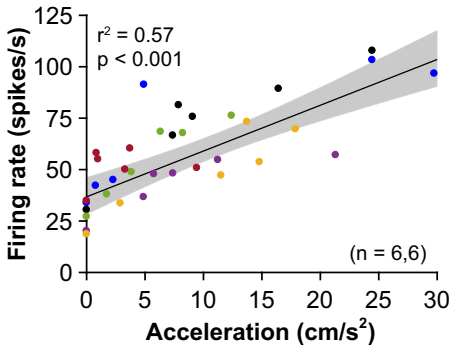

Figure 6. Utricular afferent fiber activities were positively correlated (r^2 = 0.57) with self-generated swimming events. Utricular afferent fiber firing rates (spikes/s) are plotted against swimming acceleration (cm/s^2). Spontaneous fiber activity is plotted at 0 acceleration (cm/s^2). Each data point represents an individual self-generated swimming event (n = 5/fish), and each color represents a different utricular fiber. The black line represents the best fit line, whereas the shaded region represents the 95% confidence interval. The number of animals and utricular afferents recorded is indicated in the parentheses.

responses to passive and active movements yet maintain sensitivity to conspecific boatwhistle vocalization playbacks.

Across vertebrates, the inner ear otolithic end organs are thought to primarily serve a vestibular function as they detect translational movements and maintain static balance; however, they also detect vibrations at auditory frequencies [e.g., fish (5), frogs (60, 61), rats (62–64), and guinea pigs (65–67)]. In teleost fishes, the utricle acts as an inertial accelerometer and responds to direct displacement by acoustic particle motion and linear accelerations primarily in the horizontal plane (5, 7, 68). Although the saccule and lagena are considered the main auditory end organs responsible for sound detection and directional hearing in fishes (69–71), the utricle is thought to primarily serve a vestibular role acting as a gravistatic organ (35, 46, 47). These vestibular functions are supported by the utricle's dense projections to the tangential octaval nuclei, a posited vestibular brain region that also receives input from the semicircular canals (49, 72–74).

Here, we show that toadfish utricular afferents are sensitive to a range of pure tone frequencies that correspond to the fundamental frequency of male vocalizations (Fig. 3*A*) and playbacks of male courtship vocalizations (Fig. 3*C*). These results confirm previous physiological studies in batrachoid fishes (toadfish and midshipman), which have shown that utricular hair cells (48) and afferents (37) serve an auditory function and are sensitive to a broad range of behaviorally relevant acoustic frequencies, including playbacks of conspecific courtship vocalizations. Additional support for the utricle's auditory function is provided by previous neuroanatomical studies, which have shown that utricular primary afferents of batrachoid fishes project centrally to the intermediate, rostral intermediate, and dorsolateral auditory zones of the hindbrain descending octaval nucleus (DON) and the auditory region of the midbrain torus semicircularis, similar to the saccule and lagena (49, 75). The auditory role of the utricle is further supported by neuroanatomical and physiological evidence in the sleeper goby *(Dormitator latifrons)*, which along with the saccule and lagena projects centrally to the intermediate auditory zone of the DON (74) and is directionally sensitive to auditory stimuli (59, 76, 77). Together, this study and previous studies strongly suggest that the utricle of batrachoid fishes, and other fishes, serves an auditory function and can encode auditory information.

Consistent with the otolithic end organs functioning as linear accelerometers that transduce translational movements, we show that both slow and fast adapting utricular afferent fibers exhibit increased firing rates (spikes/s) during movements (Figs. 4 and 6). These increased activity levels are consistent with previous studies in the toadfish, which demonstrated robust utricular responses during passive yaw rotations (34), sinusoidal linear movements (35), and active gilling movements (37). Since toadfish are benthic ambush predators that primarily exhibit short-distance swimming bouts ($\sim$ 2 m) ranging from 3.5 to 18.6 cm/s interspersed by stationary periods (42, 78), we utilized passive movements to control for a range of behaviorally relevant swimming speeds. We observed that increased utricular afferent activity levels (spikes/s) correspond to increasing passive movement accelerations, which in turn were correlated with increased particle acceleration levels (dB re: 1 m/s^2). While the in vivo electrophysiology approach used in the present study did not allow for determining the mechanisms that led to the differential adaptation of utricular afferent fibers during sustained movements, passive and active movement speeds failed to saturate any of the afferent fibers. Taken together, these results show that utricular afferents encode a range of behaviorally relevant linear accelerations during both passive and active movements.

The variability in swimming motivation, speed, and direction made it difficult for fish to consistently approach the underwater acoustic source at the same angle and speed.

Figure 5. Utricular afferent activity increases in response to boatwhistle playbacks during slow passive movements. *A* and *B*: utricular afferent firing rates (spikes/s) of a slow (TF18-B) and fast (TF26-A) adapting fiber during slow passive movement when boatwhistle acoustic stimuli are *i*) absent and *ii*) present. Each panel from top to bottom displays the utricular fiber firing rate (spikes/s), auditory stimulus, velocity (cm/s), and acceleration (cm/s^2). The shaded gray regions indicate when fish were passively moved. *Aiii* and *Biii*: polar plots of utricular afferent vector strength, or the coefficient of synchronization (*R*), in response to boatwhistle playbacks (n = 10) during slow passive movement. Vector strength, which is plotted along concentric lines, is plotted along the angle of the speaker relative to the fish before, during (initial, middle, and end), and after passive movements. *C*: utricular afferent firing rates (spikes/s) while stationary (Spontaneous), during boatwhistle playbacks while stationary (Boatwhistle), slow passive movements (Slow), and in response to boatwhistle vocalization playbacks during slow movement (Boatwhistle + Slow). Bar graphs represent the means ± SD of each group across all trials conducted, while open circles represent utricular afferent firing rates for each trial. Different letters (a, b, c, and d) indicate significantly different utricular afferent firing rates (spikes/s) between various stimuli presented (pairwise comparison with Holm correction, $P < 0.05$). The parentheses indicate the number of animals and utricular afferent fibers recorded. *D*: boxplots of particle acceleration levels (dB re: 1 m/s^2) during boatwhistle playbacks (Boatwhistle) and slow passive movements when boatwhistles were absent (Slow) and present (Boatwhistle + Slow). Control indicates the background particle acceleration levels (dB re: 1 m/s^2) within the experimental arena when all stimulus was absent. Data median is represented by the horizontal line within each box and the mean of the data by an open circle. The box extends to the 25th and 75th percentile, while the upper and lower tails extend to the 90th and 10th percentiles, respectively.

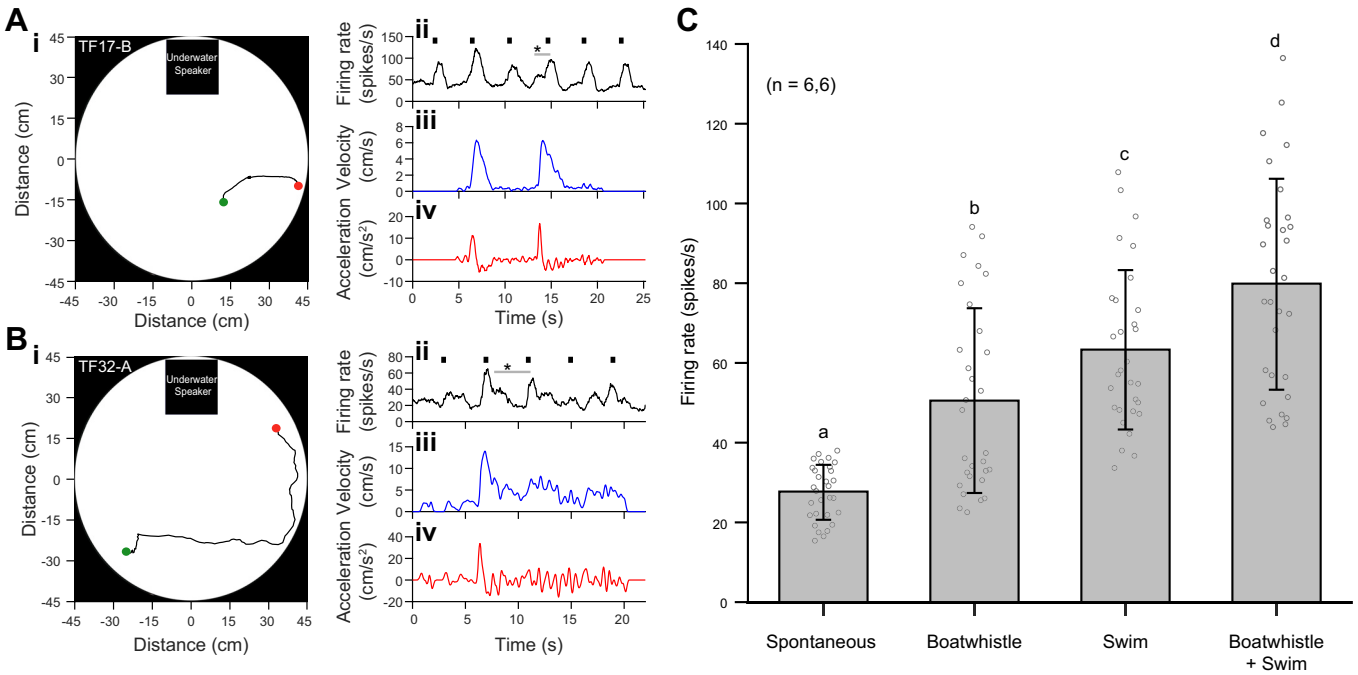

Figure 7. Utricular auditory sensitivity during swimming. Representative fast (TF17-B) (*A*) and slow (TF32-A) (*B*) adapting utricular afferent fiber activities in response to boatwhistle playbacks during swimming. For both *A* and *B*: *i*) experimental arena, where black lines represent the path of toadfish movement during each swimming event from the start (green circle) to the end of movement (red circle). The black box indicates the position of the underwater speaker during experimental trials. *ii*) Utricular afferent firing rates (spikes/s) of swimming toadfish in response to boatwhistle playbacks. The thick black bars above the firing rates indicate when boatwhistle playbacks occurred. *iii*) Instantaneous linear velocity (cm/s; blue) and *iv*) acceleration (cm/s^2; red) during self-generated swimming. *C*: utricular afferent firing rates (spikes/s) while stationary (Spontaneous), during boatwhistle playbacks while stationary (Boatwhistle), swimming (Swim), and in response to boatwhistle playbacks while swimming (Boatwhistle + Swim). Bar graphs represent the means ± SD of each group across all trials conducted, while open circles represent utricular afferent firing rates for each trial. Different letters (a, b, c, and d) indicate significantly different utricular afferent firing rates (spikes/s) between various stimuli presented (pairwise comparison with Holm correction, $P < 0.05$). The numbers in parentheses indicate the number of animals and utricular afferent fibers recorded for each group.

Therefore, in addition to allowing toadfish to swim within the experimental arena freely, fish were passively moved via a sled at behaviorally relevant swimming speeds, which allowed for a precise correlation of utricular activity (spikes/s) with speed and distance from the underwater speaker. During both passive and active movements, our results indicate that utricular afferent firing rates were not saturated during movement as acoustic stimuli increased afferent fiber firing rates (spikes/s) above evoked levels due to movement alone (Figs. 5 and 7). Fast adapting fibers were well suited to detect acoustic stimuli as the firing rates (spikes/s) of these neurons rapidly returned to rates near (±5%) spontaneous levels, thus remaining sensitive to auditory stimuli, whereas slow adapting fibers, which partially adapted during movement, were also sensitive to subsequent acoustic stimuli. In addition, phase-locking (*R*) analysis, which is a well-established approach for determining how well auditory-sensitive afferents encode the temporal characteristics of acoustic stimuli (56–58, 79), revealed that phase-locking persisted through movement. However, slow adapting neurons exhibited a decrease in *R* strength during movements, which may be due to the directional sensitivity of utricular afferent hair cells to the auditory stimuli, with differences in *R* strength resulting from differences in the orientation of the toadfish inner ear relative to the underwater sound source during movement.

It has remained unclear how fishes integrate multimodal sensory inputs, such as detecting external auditory stimuli while actively swimming. Possible mechanisms that would allow for sustained exafference sensitivity during movement are the feed-forward, predictive signaling mechanisms corollary discharge , and efference copies, which allow organisms to disambiguate reafferent and exafferent inputs via intrinsic neural representations of self-generated motor commands (80). Previously in aquatic organisms, it has been observed that predictive signaling minimizes or abolishes neural activation during the production of motor commands at various levels of sensory processing (13, 15, 19, 20, 24, 25, 81–84). For example, in the lateral line, efferent modulation has been noted during gilling (20), fictive swimming (24, 25, 84), visual stimuli (27), and fictive sound production (18). In the inner ear, efferent modulation has been observed in the saccule during fictive sound production (18) and the semicircular canals during sinusoidal mechanical indentation (17, 29) and electrical stimulation (14). Although these previous studies provided an in-depth understanding of how predictive signaling modulates afferent fiber activities, all were investigated with decerebrated (15, 20, 84), restrained (13, 14, 17, 18, 24, 25, 81, 82), or stationary (27, 85) animals receiving a single stimulus, which does not accurately reflect naturalistic behaviors. In our study, the modulation of primary afferents via predictive signaling mechanisms, which has previously been observed in the lateral line of fictive swimming zebrafish (24, 25) and inner ear of larval *Xenopus* (82), may have immediately reduced the activity of fast adapting

fibers and partially decreased the sensitivity of slow adapting fibers in free-swimming toadfish. However, if motor command outputs are necessary to modulate efferent neurons, different results would have been expected in toadfish that were moved passively versus free-swimming, yet, both passive and active swimming showed the same outcome. One possible explanation for the absence of efferent modulation in the present study may be due to the fact that rhythmicity in motor outputs is required for the generation of precise efferent copies (82, 86). Yet, as shown here, no evidence of efferent modulation was noted in toadfish anterior lateral line neurons during swimming (42). In addition, previous studies have noted that toadfish utricular efferents were not modulated by sinusoidal linear acceleration (35), auditory stimuli, or gilling (37). Although results from the present study indicate that utricular afferent fibers retain exafference sensitivity during self-generated movements, future studies that simultaneously monitor efferent activity during sustained rhythmic motor activity should be conducted in free-swimming fish to determine how predictive signaling mechanisms aid in sensory processing.

Although this study assessed utricular auditory and vestibular activity during passive and self-generated movements, several limitations should be considered. For example, the tank size (90 cm diameter) limited long-range movements and may have affected the integrity of the acoustical stimulus by producing echoes and reverberations inside the tank (87). However, utricular afferent fibers responded in phase to both pure tones and boatwhistle vocalization playbacks and ceased quickly after stimulus cessation, indicating the fidelity of the boatwhistle was maintained despite the small tank limitations. In addition, the orientation of toadfish relative to the sound source during passive and active swimming trials may have influenced utricular afferent activity due to the directional sensitivity of utricular afferent fibers or changes in sound pressure levels throughout the tank. However, sound pressure levels remained relatively uniform throughout the tank, varying only by ~2 dB re: 1 μPa along the length of the sled track and no more than 4 dB re: 1 μPa in areas the fish freely swam. Future experiments in larger tanks or in the field can more accurately address sound detection range and better represent particle motion gradients as fish approach sound sources. Furthermore, chronic neural recordings, which entail inserting electrodes into the cranial nerves or the brain, preferentially allow for isolating and recording neural activity from the largest fibers within the nerve bundle and often omits many smaller, harder to isolate fibers. Moreover, the low abundance of efferent fibers (<10% fibers) in the VIIIth nerve made it challenging to isolate sufficient fibers for statistical analysis. Several efferent fibers were located and failed to respond to table movements or tactile stimulation and were not pursued further. Future studies will target these fibers for implants to determine how they respond to self-generated and auditory stimuli in free-swimming fish.

DATA AVAILABILITY

The data that support the findings of this study are available from the corresponding author upon reasonable request. Micromanipulator .stl files can be accessed at https://github.com/LoranzieRogers/micromanipulator-files.

ACKNOWLEDGMENTS

The authors acknowledge the Marine Resources Center staff at the Marine Biological Laboratory for providing toadfish care. The authors also acknowledge Dr. Joseph Sisneros for helpful comments on the manuscript, Dr. Geoffrey Boynton for statistical consultation, and Dr. Steve Zottoli for providing the image of the toadfish brain and inner ear used in Fig. 1*B*.

Present address of L. S. Rogers: Dept. of Psychology, University of Washington, Seattle, WA 98195 (e-mail: loranzie@uw.edu).

GRANTS

Funding was provided by National Science Foundation Grants IOS 1354745 and DBI 1359230 & 1659604 (to A. F. Mensinger) and by the National Science Foundation Graduate Research Fellowship Program DGE 1762114 (to L. S. Rogers). All experimental procedures conformed to NIH guidelines for animal care and use of animals and were approved by the Marine Biological Laboratories Institutional Animal Care and Use Committee.

DISCLOSURES

No conflicts of interest, financial or otherwise, are declared by the authors.

AUTHOR CONTRIBUTIONS

L.S.R., J.C.V.W., and A.F.M. conceived and designed research; L.S.R. and J.C.V.W. performed experiments; L.S.R. analyzed data; L.S.R. and A.F.M. interpreted results of experiments; L.S.R. prepared figures; L.S.R. drafted manuscript; L.S.R., J.C.V.W., and A.F.M. edited and revised manuscript; L.S.R., J.C.V.W., and A.F.M. approved final version of manuscript.

ENDNOTE

At the request of the authors, readers are herein alerted to the fact that additional materials related to this manuscript may be found at https://github.com/LoranzieRogers/micromanipulator-files. These materials are not a part of this manuscript and have not undergone peer review by the American Physiological Society (APS). APS and the journal editors take no responsibility for these materials, for the website address, or for any links to or from it.

REFERENCES

1. **Baird IL.** Anatomical features of the inner ear in submammalian vertebrates. In: *Auditory System: Anatomy Physiology (Ear)*, edited by Ades HW, Axelsson A, Baird IL, Békésy Gv, Boord RL, Campbell CBG, Densert O, Eldredge DH, Engström H, Fex J, Harrison JM, Henson OW, Howe ME, Iurato S, Michelsen A, Møller AR, Pfeiffer RR, Rauch S, Rauch I, Shaw EAG, Wersäll J, Wever EG, Keidel WD, Neff WD. Heidelberg, Berlin: Springer, 1974, p. 159–212.
2. **Manley GA.** *Peripheral Hearing Mechanisms in Reptiles and Birds*. Berlin: Springer-Verlag, 1990.
3. **Manley GA**, **Clack JA.** An outline of the evolution of vertebrate hearing organs. In: *Evolution of the Vertebrate Auditory System*, edited by Manley GA, Popper AN, Fay RR. New York, NY: Springer, 2004, p. 1–26.
4. **Wever EG.** The evolution of vertebrate hearing. In: *Auditory System: Anatomy Physiology (Ear)*, edited by Ades HW, Axelsson A, Baird IL, Békésy Gv, Boord RL, Campbell CBG, Densert O, Eldredge DH, Engström H, Fex J, Harrison JM, Henson OW, Howe ME, Iurato S, Michelsen A, Møller AR, Pfeiffer RR, Rauch S, Rauch I, Shaw EAG, Wersäll J, Wever EG, Keidel WD, Neff WD. Heidelberg, Berlin: Springer, 1974, p. 423–454.

5. **Fay RR.** The goldfish ear codes the axis of acoustic particle motion in three dimensions. *Science* 225: 951–954, 1984. doi:10.1126/science.6474161.
6. **Platt C**, **Popper AN.** Fine structure and function of the ear. In: *Hearing and Sound Communication in Fishes*, edited by Tavolga WN, Popper AN, Fay RR. New York: Springer, 1981, p. 3–38.
7. **Popper AN**, **Fay RR.** Sound detection and processing by fish: critical review and major research questions (Part 1 of 2). *Brain Behav Evol* 41: 14–25, 1993. doi:10.1159/000113821.
8. **Schulz-Mirbach T**, **Ladich F**, **Plath M**, **Heß M.** Enigmatic ear stones: what we know about the functional role and evolution of fish otoliths. *Biol Rev Camb Philos Soc* 94: 457–482, 2019. doi:10.1111/brv.12463.
9. **Holt JC**, **Lysakowski A**, **Goldberg JM.** The efferent vestibular system. In: *Auditory and Vestibular Efferents*, edited by Ryugo DK, Fay RR, Popper AN. New York: Springer, 2010, p. 135–186.
10. **Köppl C.** Evolution of the octavolateral efferent system. In: *Auditory and Vestibular Efferents*, edited by Ryugo DK, Fay RR, Popper AN. New York: Springer, 2010, p. 217–259.
11. **Poppi LA**, **Holt JC**, **Lim R**, **Brichta AM.** A review of efferent cholinergic synaptic transmission in the vestibular periphery and its functional implications. *J Neurophysiol* 123: 608–629, 2020. doi:10.1152/jn.00053.2019.
12. **Sienknecht UJ**, **Köppl C**, **Fritzsch B.** Evolution and development of hair cell polarity and efferent function in the inner ear. *Brain Behav Evol* 83: 150–161, 2014. doi:10.1159/000357752.
13. **Boyle R**, **Rabbitt RD**, **Highstein SM.** Efferent control of hair cell and afferent responses in the semicircular canals. *J Neurophysiol* 102: 1513–1525, 2009. doi:10.1152/jn.91367.2008.
14. **Boyle R**, **Highstein SM.** Efferent vestibular system in the toadfish: action upon horizontal semicircular canal afferents. *J Neurosci* 10: 1570–1582, 1990. doi:10.1523/JNEUROSCI.10-05-01570.1990.
15. **Highstein SM**, **Baker R.** Action of the efferent vestibular system on primary afferents in the toadfish, *Opsanus tau*. *J Neurophysiol* 54: 370–384, 1985. doi:10.1152/jn.1985.54.2.370.
16. **Castellano-Muñoz M**, **Israel SH**, **Hudspeth AJ.** Efferent control of the electrical and mechanical properties of hair cells in the bullfrog's sacculus. *PLoS One* 5: e13777, 2010. doi:10.1371/journal.pone.0013777.
17. **Rabbitt RD**, **Boyle R**, **Highstein SM**, **Bennett MVL.** Mechanical amplification by hair cells in the semicircular canals. *Proc Natl Acad Sci USA* 107: 3864–3869, 2010. doi:10.1073/pnas.0906765107.
18. **Weeg MS**, **Land BR**, **Bass AH.** Vocal pathways modulate efferent neurons to the inner ear and lateral line. *J Neurosci* 25: 5967–5974, 2005. doi:10.1523/JNEUROSCI.0019-05.2005.
19. **Bell C**, **Bodznick D**, **Montgomery J**, **Bastian J.** The generation and subtraction of sensory expectations within cerebellum-like structures. *Brain Behav Evol* 50: 17–31, 1997. doi:10.1159/000113352.
20. **Montgomery JC**, **Bodznick D.** An adaptive filter that cancels self-induced noise in the electrosensory and lateral line mechanosensory systems of fish. *Neurosci Lett* 174: 145–148, 1994. doi:10.1016/0304-3940(94)90007-8.
21. **Odstrcil I**, **Petkova MD**, **Haesemeyer M**, **Boulanger-Weill J**, **Nikitchenko M**, **Gagnon JA**, **Oteiza P**, **Schalek R**, **Peleg A**, **Portugues R**, **Lichtman JW**, **Engert F.** Functional and ultrastructural analysis of reafferent mechanosensation in larval zebrafish. *Curr Biol* 32: 176–189.e5, 2022. doi:10.1016/j.cub.2021.11.007.
22. **Perks KE**, **Krotinger A**, **Bodznick D.** A cerebellum-like circuit in the lateral line system of fish cancels mechanosensory input associated with its own movements. *J Exp Biol* 223: jeb204438, 2020. doi:10.1242/jeb.204438.
23. **Flock Å**, **Russell IJ.** The post-synaptic action of efferent fibres in the lateral line organ of the burbot *Lota*. *J Physiol* 235: 591–605, 1973. doi:10.1113/jphysiol.1973.sp010406.
24. **Lunsford ET**, **Skandalis DA**, **Liao JC.** Efferent modulation of spontaneous lateral line activity during and after zebrafish motor commands. *J Neurophysiol* 122: 2438–2448, 2019. doi:10.1152/jn.00594.2019.
25. **Pichler P**, **Lagnado L.** Motor behavior selectively inhibits hair cells activated by forward motion in the lateral line of zebrafish. *Curr Biol* 30, 150–157.e3, 2020. doi:10.1016/j.cub.2019.11.020.
26. **Roberts BL**, **Russell IJ.** The activity of lateral-line efferent neurons in stationary and swimming dogfish. *J Exp Biol* 57: 435–448, 1972. doi:10.1242/jeb.57.2.435.
27. **Tricas TC**, **Highstein SM.** Action of the octavolateralis efferent system upon the lateral line of free-swimming toadfish, *Opsanus tau*. *J Comp Physiol A* 169: 25–37, 1991. doi:10.1007/BF00198170.
28. **Boyle R**, **Highstein SM.** Resting discharge and response dynamics of horizontal semicircular canal afferents of the toadfish, *Opsanus tau*. *J Neurosci* 10: 1557–1569, 1990. doi:10.1523/JNEUROSCI.10-05-01557.1990.
29. **Rabbitt RD**, **Boyle R**, **Highstein SM.** Sensory transduction of head velocity and acceleration in the toadfish horizontal semicircular canal. *J Neurophysiol* 72: 1041–1048, 1994. doi:10.1152/jn.1994.72.2.1041.
30. **Rabbitt RD**, **Boyle R**, **Highstein SM.** Mechanical indentation of the vestibular labyrinth and its relationship to head rotation in the toadfish, *Opsanus tau*. *J Neurophysiol* 73: 2237–2260, 1995. doi:10.1152/jn.1995.73.6.2237.
31. **Edds-Walton PL**, **Fay RR**, **Highstein SM.** Dendritic arbors and central projections of physiologically characterized auditory fibers from the saccule of the toadfish, *Opsanus tau*. *J Comp Neurol* 411: 212–238, 1999. doi:10.1002/(SICI)1096-9861(19990823)411:2<212::AID-CNE4>3.0.CO;2-X.
32. **Fay RR**, **Edds-Walton PL.** Directional response properties of saccular afferents of the toadfish, *Opsanus tau*. *Hear Res* 111: 1–21, 1997. doi:10.1016/S0378-5955(97)00083-X.
33. **Fay RR**, **Edds-Walton PL.** Diversity in frequency response properties of saccular afferents of the toadfish, *Opsanus tau*. *Hear Res* 113: 235–246, 1997. doi:10.1016/S0378-5955(97)00148-2.
34. **Boyle R**, **Mensinger AF**, **Yoshida K**, **Usui S**, **Intravaia A**, **Tricas T**, **Highstein SM.** Neural readaptation to earth's gravity following return from space. *J Neurophysiol* 86: 2118–2122, 2001. doi:10.1152/jn.2001.86.4.2118.
35. **Boyle R**, **Popova Y**, **Varelas J.** Influence of magnitude and duration of altered gravity and readaptation to 1 g on the structure and function of the utricle in toadfish. *Front Physiol* 9: 1469, 2018. doi:10.3389/fphys.2018.01469.
36. **Boyle R**, **Ehsanian R**, **Mofrad A**, **Popova Y**, **Varelas J.** Morphology of the utricular otolith organ in the toadfish, *Opsanus tau*. *J Comp Neurol* 526: 1571–1588, 2018. doi:10.1002/cne.24429.
37. **Maruska KP**, **Mensinger AF.** Directional sound sensitivity in utricular afferents in the toadfish *Opsanus tau*. *J Exp Biol* 218: 1759–1766, 2015. doi:10.1242/jeb.115345.
38. **Fine ML.** Seasonal and geographical variation of the mating call of the oyster toadfish *Opsanus tau* L. *Oecologia* 36: 45–57, 1978. doi:10.1007/BF00344570.
39. **Fish JF.** The effect of sound playback on the toadfish. In: *Behavior of Marine Animals: Current Perspectives in Research Volume 2: Vertebrates*, edited by Winn HE, Olla BL. New York, NY: Springer, 1972, p. 386–434.
40. **Gray G-A**, **Winn HE.** Reproductive ecology and sound production of the toadfish, *Opsanus tau*. *Ecology* 42: 274–282, 1961. doi:10.2307/1932079.
41. **Cardinal EA**, **Radford CA**, **Mensinger AF.** Potential role of the anterior lateral line in sound localization in toadfish (*Opsanus tau*). *J Exp Biol* 221: jeb180679, 2018. doi:10.1242/jeb.180679.
42. **Mensinger AF**, **Wert JCV**, **Rogers LS.** Lateral line sensitivity in free-swimming toadfish *Opsanus tau*. *J Exp Biol* 222: jeb190587, 2019. doi:10.1242/jeb.190587.
43. **Radford CA**, **Mensinger AF.** Anterior lateral line nerve encoding to tones and play-back vocalisations in free-swimming oyster toadfish, *Opsanus tau*. *J Exp Biol* 217: 1570–1579, 2014. doi:10.1242/jeb.092510.
44. **Rogers LS**, **Van Wert JC**, **Mensinger AF.** An implantable two axis micromanipulator made with a 3D printer for recording neural activity in free-swimming fish. *J Neurosci Methods* 288: 29–33, 2017. doi:10.1016/j.jneumeth.2017.06.012.
45. **Bianco IH**, **Ma L-H**, **Schoppik D**, **Robson DN**, **Orger MB**, **Beck JC**, **Li JM**, **Schier AF**, **Engert F**, **Baker R.** The tangential nucleus controls a gravito-inertial vestibulo-ocular reflex. *Curr Biol* 22: 1285–1295, 2012. doi:10.1016/j.cub.2012.05.026.
46. **Inoue M**, **Tanimoto M**, **Oda Y.** The role of ear stone size in hair cell acoustic sensory transduction. *Sci Rep* 3: 2114, 2013. doi:10.1038/srep02114.
47. **Riley BB**, **Moorman SJ.** Development of utricular otoliths, but not saccular otoliths, is necessary for vestibular function and survival in zebrafish. *J Neurobiol* 43: 329–337, 2000. doi:10.1002/1097-4695(20000615)43:4<329::AID-NEU2>3.0.CO;2-H.
48. **Rogers LS**, **Sisneros JA.** Auditory evoked potentials of utricular hair cells in the plainfin midshipman, *Porichthys notatus*. *J Exp Biol* 223, 2020. doi:10.1242/jeb.226464.

49. **Highstein SM**, **Kitch R**, **Carey J**, **Baker R.** Anatomical organization of the brainstem octavolateralis area of the oyster toadfish, *Opsanus tau*. *J Comp Neurol* 319: 501–518, 1992. doi:10.1002/cne.903190404.
50. **Highstein SM**, **Baker R.** Organization of the efferent, vestibular nuclei and nerves of the toadfish, *Opsanus tau*. *J Comp Neurol* 243: 309–325, 1986. doi:10.1002/cne.902430303.
51. **Palmer LM**, **Mensinger AF.** Effect of the anesthetic tricaine (MS-222) on nerve activity in the anterior lateral line of the oyster toadfish, *Opsanus tau*. *J Neurophysiol* 92: 1034–1041, 2004. doi:10.1152/jn.01151.2003.
52. **Colleye O**, **Vetter BJ**, **Mohr RA**, **Seeley LH**, **Sisneros JA.** Sexually dimorphic swim bladder extensions enhance the auditory sensitivity of female plainfin midshipman fish, *Porichthys notatus*. *J Exp Biol* 222: jeb204552, 2019. doi:10.1242/jeb.204552.
53. **Vetter BJ**, **Sisneros JA.** Swim bladder enhances lagenar sensitivity to sound pressure and higher frequencies in female plainfin midshipman (*Porichthys notatus*). *J Exp Biol* 223, 2020. doi:10.1242/jeb.225177.
54. **Vasconcelos RO**, **Fonseca PJ**, **Amorim MCP**, **Ladich F.** Representation of complex vocalizations in the Lusitanian toadfish auditory system: evidence of fine temporal, frequency and amplitude discrimination. *Proc R Soc London B: Biol Sci* 278: 826–834, 2011. doi:10.1098/rspb.2010.1376.
55. **Wysocki LE**, **Codarin A**, **Ladich F**, **Picciulin M.** Sound pressure and particle acceleration audiograms in three marine fish species from the Adriatic Sea. *J Acoust Soc Am* 126: 2100–2107, 2009. doi:10.1121/1.3203562.
56. **Goldberg JM**, **Brown PB.** Response of binaural neurons of dog superior olivary complex to dichotic tonal stimuli: some physiological mechanisms of sound localization. *J Neurophysiol* 32: 613–636, 1969. doi:10.1152/jn.1969.32.4.613.
57. **Lu Z**, **Fay RR.** Acoustic response properties of single units in the torus semicircularis of the goldfish, *Carassius auratus*. *J Comp Physiol A* 173: 33–48, 1993. doi:10.1007/BF00209616.
58. **Lu Z**, **Fay RR.** Acoustic response properties of single neurons in the central posterior nucleus of the thalamus of the goldfish, *Carassius auratus*. *J Comp Physiol A* 176: 747–760, 1995. doi:10.1007/BF00192623.
59. **Lu Z**, **Xu Z**, **Buchser WJ.** Coding of acoustic particle motion by utricular fibers in the sleeper goby, *Dormitator latifrons*. *J Comp Physiol A* 190: 923–938, 2004. doi:10.1007/s00359-004-0550-3.
60. **Cortopassi KA**, **Lewis ER.** High-frequency tuning properties of bullfrog lagenar vestibular afferent fibers. *J Vestib Res* 6: 105–119, 1996.
61. **Cortopassi KA**, **Lewis ER.** A comparison of the linear tuning properties of two classes of axons in the bullfrog lagena. *Brain Behav Evol* 51: 331–348, 1998. doi:10.1159/000006546.
62. **Huang J**, **Tang X**, **Xu Y**, **Zhang C**, **Chen T**, **Yu Y**, **Mustain W**, **Allison J**, **Iversen MM**, **Rabbitt RD**, **Zhou W**, **Zhu H.** Differential activation of canal and otolith afferents by acoustic tone bursts in rats. *J Assoc Res Otolaryngol* 23: 435–453, 2022. [Erratum in *J Assoc Res Otolaryngol* 23: 45, 2022]. doi:10.1007/s10162-022-00839-1.
63. **Zhu H**, **Tang X**, **Wei W**, **Mustain W**, **Xu Y**, **Zhou W.** Click-evoked responses in vestibular afferents in rats. *J Neurophysiol* 106: 754–763, 2011. doi:10.1152/jn.00003.2011.
64. **Zhu H**, **Tang X**, **Wei W**, **Maklad A**, **Mustain W**, **Rabbitt R**, **Highstein S**, **Allison J**, **Zhou W.** Input–output functions of vestibular afferent responses to air-conducted clicks in rats. *J Assoc Res Otolaryngol* 15: 73–86, 2014. doi:10.1007/s10162-013-0428-6.
65. **Curthoys IS**, **Vulovic V**, **Sokolic L**, **Pogson J**, **Burgess AM.** Irregular primary otolith afferents from the guinea pig utricular and saccular maculae respond to both bone conducted vibration and to air conducted sound. *Brain Res Bull* 89: 16–21, 2012. doi:10.1016/j.brainresbull.2012.07.007.
66. **Curthoys IS**, **Burgess AM**, **Goonetilleke SC.** Phase-locking of irregular guinea pig primary vestibular afferents to high frequency (>250 Hz) sound and vibration. *Hear Res* 373: 59–70, 2019. [Erratum in *Hear Res* 389: 107909, 2020]. doi:10.1016/j.heares.2018.12.009.
67. **Curthoys IS**, **Vulovic V.** Vestibular primary afferent responses to sound and vibration in the guinea pig. *Exp Brain Res* 210: 347–352, 2011. doi:10.1007/s00221-010-2499-5.
68. **De Vries HL.** The mechanics of the labyrinth otoliths. *Acta Otolaryngol* 38: 262–273, 1951. doi:10.3109/00016485009118384.
69. **Hawkins AD**, **Popper AN.** Directional hearing and sound source localization by fishes. *J Acoust Soc Am* 144: 3329–3350, 2018. doi:10.1121/1.5082306.
70. **Sand O.** Directional sensitivity of microphonic potentials form the perch ear. *J Exp Biol* 60: 881–899, 1974. doi:10.1242/jeb.60.3.881.
71. **Sisneros JA**, **Rogers PH.** Directional hearing and sound source localization in fishes. In: *Fish Hearing and Bioacoustics: An Anthology in Honor of Arthur N. Popper and Richard R. Fay*, edited by Sisneros JA. Cham, Switzerland: Springer International Publishing, 2016, p. 121–155.
72. **Maruska KP**, **Tricas TC.** Central projections of octavolateralis nerves in the brain of a soniferous damselfish (*Abudefduf abdominalis*). *J Comp Neurol* 512: 628–650, 2009. doi:10.1002/cne.21923.
73. **Meredith GE**, **Butler AB.** Organization of eighth nerve afferent projections from individual endorgans of the inner ear in the teleost, *Astronotus ocellatus*. *J Comp Neurol* 220: 44–62, 1983. doi:10.1002/cne.902200106.
74. **Tomchik SM**, **Lu Z.** Octavolateral projections and organization in the medulla of a teleost fish, the sleeper goby (*Dormitator latifrons*). *J Comp Neurol* 481: 96–117, 2005. doi:10.1002/cne.20363.
75. **Sisneros JA**, **Marchaterre MA**, **Bass AH.** Otolithic endorgan projections of the inner ear in a vocal fish. *Bioacoustics* 12: 137–139, 2002. doi:10.1080/09524622.2002.9753674.
76. **Lu Z**, **Xu Z**, **Buchser WJ.** Acoustic response properties of lagenar nerve fibers in the sleeper goby, *Dormitator latifrons*. *J Comp Physiol A* 189: 889–905, 2003. doi:10.1007/s00359-003-0462-7.
77. **Lu Z**, **Xu Z**, **Buchser WJ.** Frequency coding of particle motion by saccular afferents of a teleost fish. *J Exp Biol* 213: 1591–1601, 2010. doi:10.1242/jeb.038836.
78. **Palmer LM**, **Giuffrida BA**, **Mensinger AF.** Neural recordings from the lateral line in free-swimming toadfish, *Opsanus tau*. *Biol Bull* 205: 216–218, 2003. doi:10.2307/1543260.
79. **Fettiplace R.** Hair cell transduction, tuning, and synaptic transmission in the mammalian cochlea. *Compr Physiol* 7: 1197–1227, 2017. doi:10.1002/cphy.c160049.
80. **Straka H**, **Simmers J**, **Chagnaud BP.** A new perspective on predictive motor signaling. *Curr Biol* 28: R232–R243, 2018. doi:10.1016/j.cub.2018.01.033.
81. **Chagnaud BP**, **Baker R**, **Bass AH.** Vocalization frequency and duration are coded in separate hindbrain nuclei. *Nat Commun* 2: 346, 2011. doi:10.1038/ncomms1349.
82. **Chagnaud BP**, **Banchi R**, **Simmers J**, **Straka H.** Spinal corollary discharge modulates motion sensing during vertebrate locomotion. *Nat Commun* 6: 7982, 2015. doi:10.1038/ncomms8982.
83. **Chagnaud BP**, **Bass AH.** Vocal corollary discharge communicates call duration to vertebrate auditory system. *J Neurosci* 33: 18775–18780, 2013. doi:10.1523/JNEUROSCI.3140-13.2013.
84. **Russell IJ**, **Roberts BL.** Inhibition of spontaneous lateral-line activity by efferent nerve stimulation. *J Exp Biol* 57: 77–82, 1972. doi:10.1242/jeb.57.1.77.
85. **Rabbitt RD**, **Boyle R**, **Highstein SM.** Influence of surgical plugging on horizontal semicircular canal mechanics and afferent response dynamics. *J Neurophysiol* 82: 1033–1053, 1999. doi:10.1152/jn.1999.82.2.1033.
86. **França de Barros F**, **Bacqué-Cazenave J**, **Taillebuis C**, **Courtand G**, **Manuel M**, **Bras H**, **Tagliabue M**, **Combes D**, **Lambert FM**, **Beraneck M.** Conservation of locomotion-induced oculomotor activity through evolution in mammals. *Curr Biol* 32: 453–461.e4, 2022. doi:10.1016/j.cub.2021.11.022.
87. **Rogers PH**, **Hawkins AD**, **Popper AN**, **Fay RR**, **Gray MD.** Parvulescu revisited: small tank acoustics for bioacousticians. In: *The Effects of Noise on Aquatic Life II*, edited by Popper AN, Hawkins A. New York: Springer, 2016, p. 933–941.